ACS APPLIED MATERIALS & INTERFACES

Research Article

www.acsami.org

Vertically Aligned Arrays of $BaTiO_3$ Nanowires

Zhi Zhou,[†] Haixiong Tang,[†] and Henry A. Sodano*[,†,‡]

[†]Department of Material Science and Engineering and [‡]Department of Mechanical and Aerospace Engineering, University of Florida, Gainesville, Florida 32611, United States

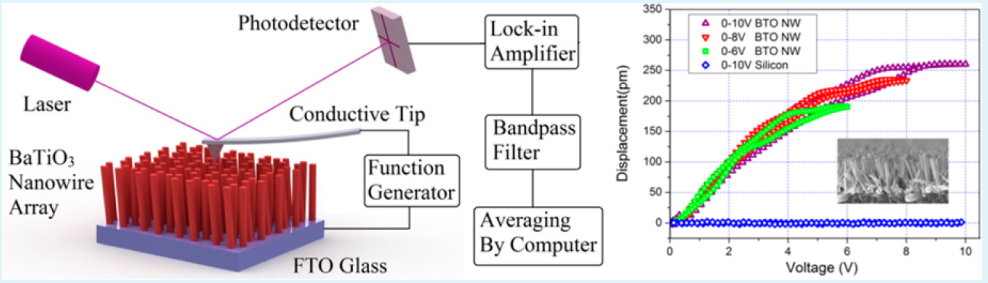

ABSTRACT: Barium titanate ($BaTiO_3$) nanowires have gained considerable research interest due to their lead-free composition and strong energy conversion efficiency. However, most research has focused on free-standing $BaTiO_3$ nanowires, which are hard to apply for sensing and energy harvesting. Here, a novel method for the growth of vertically aligned $BaTiO_3$ nanowire arrays on a conductive substrate is developed, and their electromechanical coupling behavior is directly evaluated to yield the strain coupling coefficient. The preparation of vertically aligned $BaTiO_3$ nanowire arrays is based on a two-step hydrothermal reaction by first growing oriented rutile TiO_2 nanowire arrays and then converting them to $BaTiO_3$ while simultaneously retaining their morphology. A refined piezoelectric force microscopy (PFM) testing method is applied to demonstrate the piezoelectric behavior of $BaTiO_3$ nanowires in the longitude direction. The piezoelectric response (d_{33} = 43 ± 2 pm/V) of the $BaTiO_3$ nanowires is measured to demonstrate their potential application in sensors, energy harvesting, and micro-electromechanical systems.

KEYWORDS: *$BaTiO_3$, nanowire, vertically aligned nanowire array, piezoelectric*

INTRODUCTION

Ferroelectric materials have been applied to a vast range of sensors,[1−3] actuators,[4−6] and energy-harvesting systems[7−9] due to their strong electromechanical coupling. With the miniaturization of electric systems and the development of nanotechnology, intense experimental efforts have been spent on ferroelectric nanomaterials such as ultrathin films,[10−13] nanowires,[14,15] nanorods,[16,17] nanotubes,[18,19] and nanocubes.[20] Among these, one dimensional (1D) nanostructured materials, specifically nanowires, are the smallest dimensional structures that can be used for efficient transport of electrons and are thus expected to show high energy conversion efficiency. Additionally, the nanowires are very compliant which leads to a high sensitivity to small, random mechanical disturbances that can be utilized in harvesting energy from the environment[21,22] and sensing devices at the nanoscale.[23] However, these 1D ferroelectric nanostructures are typically synthesized in the powder form making them hard to apply in practice due to their anisotropic properties and challenges achieving uniform alignment. Compared to free-standing nanowires, vertically aligned ferroelectric nanowire arrays have shown a greater potential to be incorporated into electronic devices and nanomechanical systems.[25,26] To directly utilize the ferroelectric arrays in energy harvesting and sensors, the vertically aligned nanowires are typically grown on conductive substrates, which directly act as electrodes for the application or measurement of electric fields.[24]

The recent literature has shown the strong potential of piezoelectric nanowires primarily through the use of ZnO for sensing and energy harvesting.[27,28] However, ZnO is not a ferroelectric material and has a low electromechanical coupling coefficient, potentially reducing its performance in these applications in comparison to ferroelectrics. With the desire to grow alternative compositions of ferroelectric materials in vertically aligned arrays, Sodano et al. reported a hydrothermal process for the synthesis of lead zirconium titanate (PZT) nanowire arrays.[24] This synthesis approach was later applied by Wang et al.[29] and characterized for energy harvesting. Beyond the growth of PZT nanowire arrays, little progress has been made in the broader area of ferroelectric nanowire arrays. Here a new approach to the synthesis of ferroelectric nanowires is described, and the electromechanical coupling of the nanowires is directly measured.

Barium titanate ($BaTiO_3$) has attracted significant attention due to its strong ferroelectric properties as well as its environmental benefits compared to lead-based ceramics such as PZT.[30,31] During the past decade, $BaTiO_3$ nanowires have been widely studied because of their potential application in sensing and energy harvesting.[32−34] Unban et al. first grew single-crystalline perovskite $BaTiO_3$ nanorods using a solution-

Received: August 25, 2013
Accepted: November 5, 2013
Published: November 5, 2013

based method and showed the local nonvolatile electric polarization can be induced and repeatedly manipulated.[35] In an effort to grow arrays of $BaTiO_3$ nanostructures, Yang et al. used a TiO_2 nanotube array as a precursor and then converted them to a $BaTiO_3$ nanotube array using a hydrothermal method. However, the resulting nanotube arrays resembled porous films, while nanowire arrays typically require isolated individual wires.[24] Recently, vertically aligned arrays of ferroelectric nanowires have been reported to be grown on conductive substrates by pulsed laser deposition (PLD)[36] and hydrothermal reactions.[37,38] However, the epitaxial growth of vertically aligned nanowire arrays on conductive substrates is complicated due to the requirement of a highly oriented buffer layer. Due to their benefits in dye-sensitized solar cells, a methodology was developed for the growth of rutile TiO_2 nanowire arrays on FTO glass that showed low density and highly oriented growth.[39] In this paper, a two-step hydrothermal process is developed that utilizes these vertically aligned arrays of rutile TiO_2 nanowires as a template for the formation of aligned $BaTiO_3$ nanowire arrays. The morphology, phase composition, and ferroelectric properties are characterized leading to the direct measurement of the piezoelectric strain coefficient. A refined piezoelectric force microscopy (PFM) testing method has been developed to decrease the error in the PFM measurement allowing the coupling coefficient of the nanowires to be directly measured. The strong piezoelectric response of the nanowires demonstrates the potential to replace prior materials in sensing and energy-harvesting applications.

EXPERIMENTAL DETAILS

Preparation of the vertically aligned $BaTiO_3$ nanowire arrays is based on a two-step hydrothermal reaction. As shown in Figure 1, TiO_2 nanowire arrays were first grown on fluorine-doped tin oxide (FTO) glass (Pilkington, TEC7 coated, 2.2 mm thick, 7 Ω/sq) using a hydrothermal process.[39] The FTO glass was initially cut into a square dimension (~10 mm × ~10 mm) using a laser ablator (Epilog Laser) and cleaned by sonication for 30 min in a mixed solution of deionized water, acetone, and 2-propanol with volume ratios of 1:1:1. The FTO glass substrate was then rinsed with methanol and water and placed vertically inside a reactor containing 10 mL of deionized water, 10 mL of hydrochloric acid (Fisher, 37%), and 1 mL of titanium isopropoxide (Fisher, ACS). The reactor was then heated to 200 °C for 3 h. Following the first hydrothermal process, the reactor was cooled to room temperature, and the resultant substrate with an array of vertically aligned TiO_2 nanowires was rinsed with deionized water and dried in ambient air. The substrates were then put into a solution with Ba^{2+} ions and converted to $BaTiO_3$ by a second hydrothermal reaction. Typically, the obtained TiO_2 nanowire array was put in 20 mL of a 0.02 M $Ba(OH)_2{\cdot}8H_2O$ (Sigma-Aldrich, ACS, 98%) solution within a 50 mL Teflon-lined stainless steel autoclave with a fill factor of 0.4. The reaction vessel was kept at 210 °C for 8 h. After the hydrothermal process was complete, the nanowire array was collected and sequentially washed with a 0.2 M diluted HCl aqueous solution, water, and ethanol to yield the $BaTiO_3$ nanowire array. Lastly, samples were heated at 600 °C for 30 min to remove the hydroxyl ions and reduce the dielectric loss due to the hydrothermal reaction conditions.[40,41]

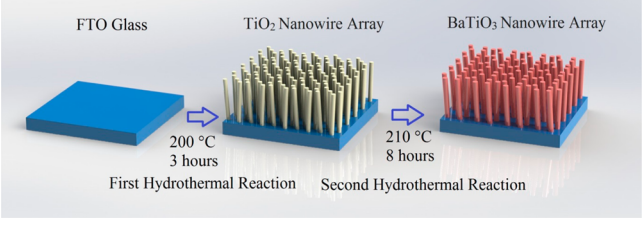

Figure 1. Schematic illustration of the growth procedure for the vertically aligned $BaTiO_3$ nanowire array.

Characterization of the sample morphology was performed by scanning electron microscopy (SEM) (6335F, JEOL). Energy-dispersive X-ray spectroscopy (EDX) (Oxford) was performed to study the chemical composition of the nanowires. X-ray diffraction (XRD) was performed on a laboratory X-ray diffractometer equipped with a curved position sensitive detector (CPS120, Inel) and a Cu Kα X-ray tube source. To characterize the surface topography of the samples, topography images of the sample surface were obtained on an atomic force microscope (AFM) (XE-70, Park Systems Co., Korea) in noncontact mode. The piezoelectric response was obtained using AFM with a conductive Ti−Pt coated tip (ATEC-NCPt, k = 42 N/m, f = 335 kHz) in a contact mode. A lock-in amplifier (Stanford Instruments SR830) was used, and an applied ac signal frequency of 17 kHz was chosen to avoid unnecessary topographic crosstalk near the cantilever resonance.

RESULTS AND DISCUSSION

The preparation of vertically aligned $BaTiO_3$ nanowire arrays is based on a two-step hydrothermal reaction. The first hydrothermal reaction produces a clean layer of TiO_2 nanowire arrays on a glass surface coated with a layer of fluorine-doped tin oxide (FTO) without cracks or precipitate on its top surface (Figure 2a and 2b). The length and the diameter of the nanowires are approximately 1 μm and 70 nm, respectively, as determined through analysis of the SEM images with ImageJ

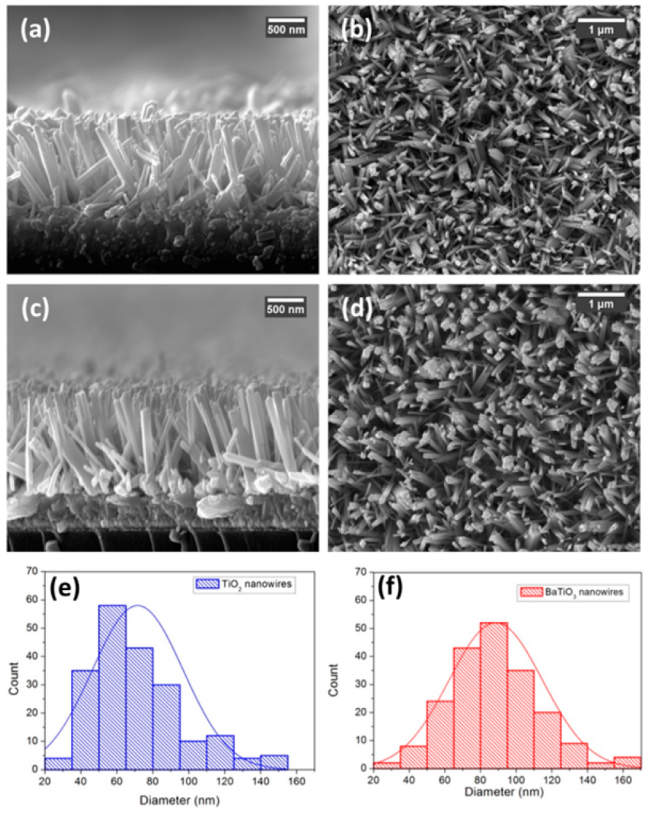

Figure 2. SEM images of TiO_2 and $BaTiO_3$ nanowires: (a) cross-sectional view of TiO_2 nanowire arrays, (b) top view of the TiO_2 nanowire arrays, (c) the cross-sectional view of $BaTiO_3$ nanowire arrays, (d) the top view of $BaTiO_3$ nanowire arrays, (e) TiO_2 nanowire diameter distribution, and (f) $BaTiO_3$ nanowire diameter distribution.

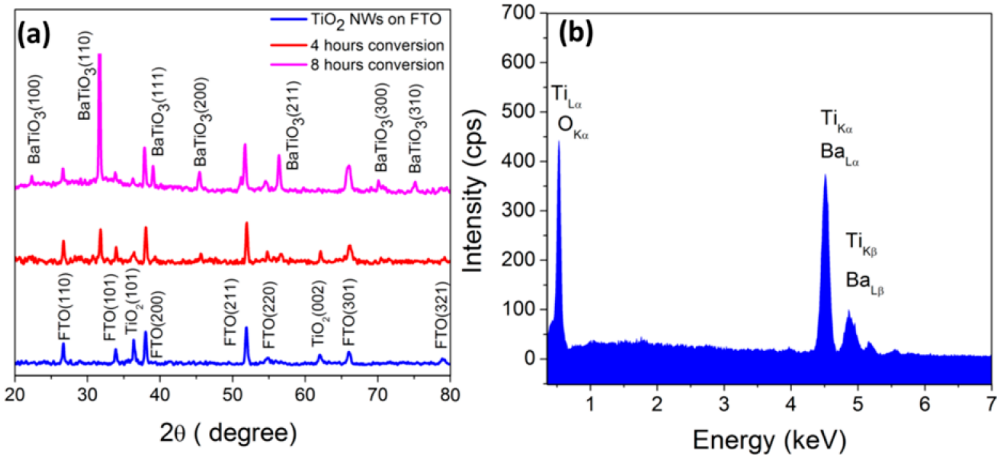

Figure 3. (a) XRD patterns of TiO_2 nanowires grown on FTO glass and $BaTiO_3$ nanowires obtained after various conversion times. (b) EDX pattern of $BaTiO_3$ nanowires.

software. It should be noted that the nanowires are vertical to the substrate surface and firmly attached even maintaining their form following ultrasonication. The epitaxial growth of TiO_2 nanowires on the FTO substrate is due to a 2% lattice mismatch between the tetragonal FTO ($a = b = 0.4687$ nm) and rutile TiO_2 ($a = b = 0.4594$ nm).[39] It can be seen in Figure 2b that the TiO_2 nanowire arrays uniformly coat the substrate and have a sufficiently large space between each nanowire to allow conversion to $BaTiO_3$ through the reaction of Ba ions with the rutile lattice. This reaction occurs through a second hydrothermal reaction in an alkaline aqueous solution with various Ba salts. To effectively convert the nanowire arrays, 0.02 M $Ba(OH)_2{\cdot}8H_2O$ was added to the solution to provide enough barium source in solution. Also, the pH value is kept around 12.5 to prevent etching of the FTO-coated glass substrate and simultaneously ensure the conversion from TiO_2 to $BaTiO_3$ while maintaining the morphology of the template arrays.[42,43]

Following conversion, the $BaTiO_3$ arrays are firmly attached to the substrate, and as shown in Figure 2c and 2d, it can be seen that the reaction preserves the nanowire morphology. The mechanism of the conversion from TiO_2 to $BaTiO_3$ during the hydrothermal reaction has been widely studied.[43−46] Typically, the process can be divided into two steps: the first step is the dissolution of the TiO_2 and the formation of $BaTiO_3$ on the surface of TiO_2, while the second step is the growth of $BaTiO_3$ via thermodynamic driving force. As shown in the reaction formulas 1 and 2, the TiO_2 is dissolved in the solution to form $Ti(OH)_4$, which subsequently reacts with the Ba ions and forms a layer of $BaTiO_3$ on the surface of the TiO_2. Subsequently, the $BaTiO_3$ crystals grow and eventually convert the whole crystal to $BaTiO_3$ with increasing reaction time.

$$TiO_2 + 2H_2O \rightarrow Ti(OH)_{4aq} \quad (1)$$

$$Ba^{2+} + Ti(OH)_{4aq} \rightarrow BaTiO_3 + 2H^+ + H_2O \quad (2)$$

On the basis of this reaction, it is expected that there should be a change in the diameter of the nanowire as the rutile lattice is converted to tetragonal $BaTiO_3$. Through an analysis of 200 separate nanowires in each SEM image, the diameter before and after conversion is shown in Figure 2e and 2f, and the mean diameter of nanowires increases from 70 to 90 nm which correlates well with the theoretical increase expected. However, the increased diameter does not lead to fusing of the arrays as was shown in prior research.[47] In addition, FTO can be utilized as the bottom electrode for testing and application of $BaTiO_3$ nanowires in the future devices. It should also be noted that this process is not limited to FTO but is universally applicable to a host of conductive or nonconductive substrates, including Ti foil, ITO glass, or Si, so long as the substrate can handle the initial hydrothermal reaction in 6 M hydrochloric acid.

To confirm the conversion of the TiO_2 nanowire arrays to $BaTiO_3$, samples are characterized by XRD as shown in Figure 3a. For the XRD pattern of the TiO_2 nanowire array grown on FTO glass, it is clearly demonstrated that the diffraction peaks from the precursor TiO_2 nanowires match well with the tetragonal rutile phase (JCPDS No. 88-1175, $a = b = 0.4517$ nm and $c = 0.2940$ nm).[39,48,49] After the second hydrothermal reaction, it is clearly shown that rutile TiO_2 nanowire arrays on FTO glass have been converted to $BaTiO_3$. With increasing conversion time, the intensity of the $BaTiO_3$ characteristic peaks increases, while that of the TiO_2 characteristic peaks decrease (Figure 3a), which indicates strong crystallization of $BaTiO_3$ nanowires. The conversion temperature and time of the second hydrothermal reaction have been optimized to maximize the conversion of the TiO_2 phase. Thus, there are strong peaks for $BaTiO_3$ along with a very small peak belonging to the residual TiO_2 phase in the nanowire arrays. Further increasing reaction time leads to the formation of $BaTiO_3$ particles which begin filling the gap between the nanowires and eventually lead to the fusing of the nanowires together and the formation of a continuous film.[47] The successful transformation of $BaTiO_3$ nanowires is further confirmed due to the presence of Ba and Ti in EDX pattern (Figure 3b). However, it should be noted that it is hard to clearly observe the separate peaks of Ba, Ti, and O. The peaks of Ba (L-edge) and Ti (K-edge) overlap in the energy range of 4.5−5 keV, and the peaks of Ti (L-edge) and O (K-edge) overlap in the energy range of 0.4−0.5 eV; thus, this alone cannot show conversion.

With this being the first demonstration of vertically aligned barium titanate nanowire arrays, it is important to understand the electromechanical properties of this new form. Piezoelectric force microscopy (PFM) is widely utilized to characterize ferroelectric nanomaterials.[50−52] However, standard PFM techniques cannot accurately identify the coupling coefficient or more specifically the piezoelectric strain coupling coefficient (d coefficient). Therefore, a refined approach is used here in

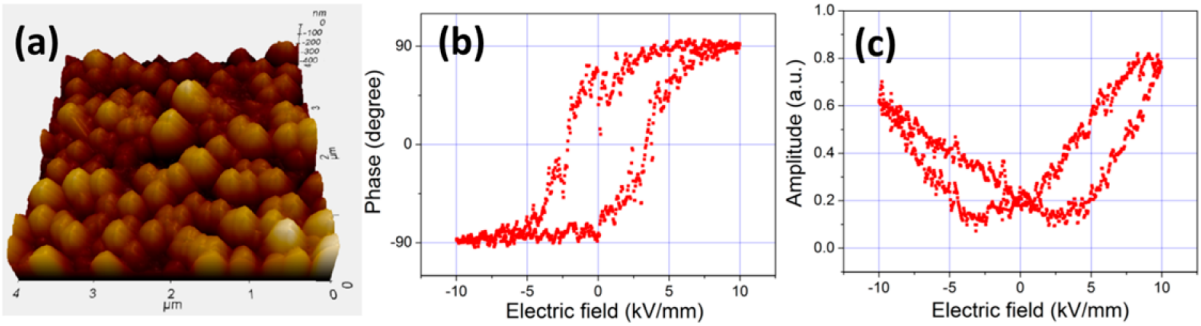

Figure 4. (a) Topography of the $BaTiO_3$ nanowires by AFM; the hysteresis loop of the $BaTiO_3$ nanowires: (b) phase and (c) amplitude.

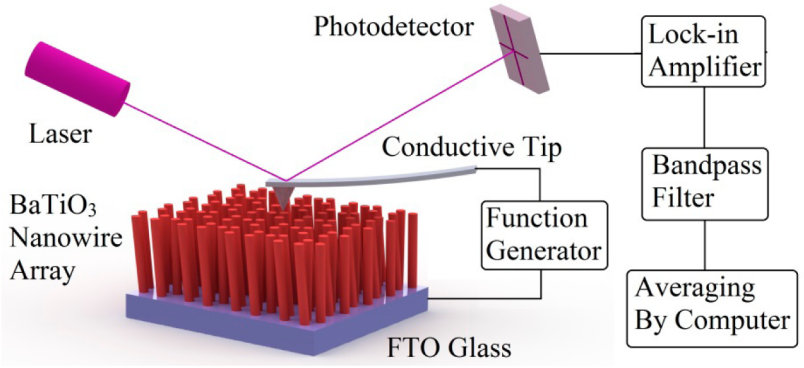

Figure 5. Schematic plot of the PFM testing.

which an AFM equipped with PFM mode is employed to study the ferroelectric behavior of the $BaTiO_3$ nanowire arrays by using the high displacement sensitivity of the AFM as a sensor and applying a filtering and averaging scheme over numerous cyclic measurements. This method takes advantage of the subnanoscale measurement capabilities of AFM, which has the ability to measure the induced deformations of nanowires due to an applied local electric field with a noise floor on the order of tens of picometers. When used with free-standing nanowires, the AFM can only apply an electric field along the radial direction of the nanowire and detect the piezoelectric response of the $BaTiO_3$ nanowire in the axis of the electric field (d_{33}) or along the length through the shear force on the tip (d_{31}) which is subject to greater uncertainty. However, the piezoelectric response along the longitudinal direction of the $BaTiO_3$ nanowires is more important to study due to the anisotropy of nanowires and potential application as nanosensors and energy harvesters. In other words, it is highly desirable to measure the strain of the nanowire with the field applied along its length and measure the corresponding strain in this direction. Since the $BaTiO_3$ nanowire arrays are vertically aligned on a conductive substrate, the piezoelectric response along the longitudinal direction of the nanowire can be measured directly with the AFM through the application of an electric field along this axis.

To demonstrate the ferroelectricity of the $BaTiO_3$ nanowires, standard PFM is first performed to characterize the ferroelectric properties of the nanowires. Initially, the conductive tip is scanned over the nanowire array to find the top facet of the nanowire. To obtain an accurate topography of the nanowire array, the scan is performed in noncontact mode at a low scan speed (0.8 μm/s) to avoid contact between the AFM tip and nanowires as shown in Figure 4a. From the surface scan, the tips of the nanowires can be identified, and the AFM tip is then placed at this location followed by switching to contact mode. An intermediate force is applied (1500 nN) to ensure that the tip deflection is dominated by the electromechanical response of the nanowire rather than electrostatic forces. The AFM tip is then used as a ground, and an excitation waveform is applied to the bottom FTO electrode to induce a piezoelectric response from the nanowire. Meanwhile, a lock-in amplifier is utilized to reduce noise in the signal displacement. The detected signal from the lock-in amplifier is comprised of the amplitude and the phase (Figure 4b and 4c), which correspond to the magnitude of the piezoelectric response and the polarization direction of the nanowires, respectively.

There is a phase change from 90° to −90° during the application of the driving signal which can be interpreted as a result of switching in the polarization direction of the nanowire (Figure 4b). As calculated from Figure 4b, the coercive field of the $BaTiO_3$ nanowires is 3 kV/mm, using an approximate nanowire length of 1 μm. In addition, the same coercive field value is obtained from the amplitude−voltage hysteresis loop (Figure 4c) which supports the data obtained from the phase−voltage hysteresis loop (Figure 4b). Furthermore, the measured amplitude hysteresis loop through the standard PFM method (Figure 4c) shows a typical butterfly loop, indicating the polarization switching and the piezoelectric effect of the $BaTiO_3$ nanowire. These results demonstrate the ferroelectricity of the $BaTiO_3$ nanowires, which further confirm the conversion from TiO_2 to $BaTiO_3$.

However, the piezoelectric strain coupling coefficient cannot be measured using standard PFM techniques since the amplitude of the signal from the lock-in amplifier is difficult to convert to the real displacement of the nanowires' top surface. Therefore, a novel technique has been developed here that measures the response over numerous cycles (>200) in the presence of a band pass filter such that the actual displacement

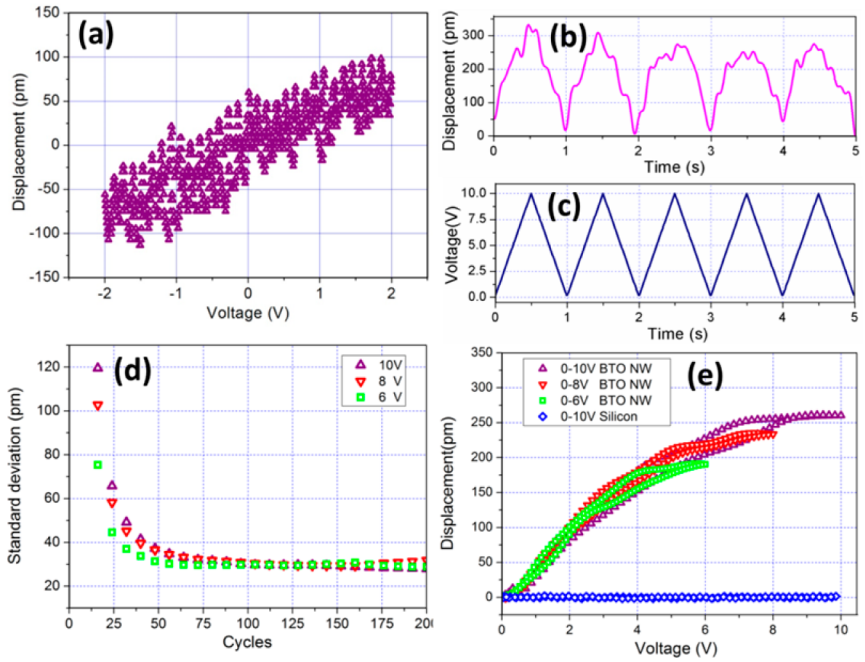

Figure 6. Piezoelectric response of the $BaTiO_3$ with PFM: (a) The displacement of the $BaTiO_3$ nanowire top surface with −2 to 2 V DC voltage; (b) the filtered displacement of the $BaTiO_3$ nanowire top surface; (c) the excitation waveform with amplitude of 10 V; (d) the standard deviation of the averaged displacement as a function of the number of cycles; (e) displacement of a $BaTiO_3$ nanowire when subjected to three unipolar excitation waveforms of varying amplitude and the absence of a displacement from silicon to demonstrate the AFM tip is not influenced by the applied field.

loop can be measured even in the presence of noise. The experimental setup of the test is schematically illustrated in Figure 5. This technique uses a 1 Hz triangle wave with varying amplitudes and records the nanowire's top surface displacement in contact mode. A similar approach has been employed by Sodano et al. along with a validation of the resulting data showing it to be accurate.[53] However, this prior study was performed on larger specimens and thus did not require filtering and averaging to reduce the measurement uncertainty. To demonstrate the technique in the presence of noise, a small amplitude bipolar triangle wave with an amplitude from −2 to 2 V, which is below the coercive field, is applied to the nanowire. Figure 6a shows the measured displacement indicating the effective piezoelectric coefficient is 35 ± 10 pm/V. As can be seen from the figure, there is considerable noise in the measured signal which generates considerable uncertainty in the measurement (approximately 30% uncertainty).

To decrease the uncertainty, 200 cycles of the displacement signals are collected and filtered with a band pass filter (Figure 6b) centered at the frequency of the applied signal with a cutoff one decade above and below, while simultaneously acquiring the excitation waveforms (Figure 6c). The surface displacement induced by the piezoelectric effect is then averaged such that the measurement error and impact of noise can be minimized. The effect of averaging on the measurement error is shown via the average of the standard deviation calculated for each data point in Figure 6d as a function of the number of displacement cycles recorded. As can be seen by the figure, the standard deviation averaged displacement decreases as the number of cycles increases and saturates at 30 pm after 100 cycles, indicating that the results are closer to the actual piezoelectric behavior by performing the filtering and averaging process. Figure 6e shows the piezoelectric behavior of $BaTiO_3$ nanowires as a function of electric field: initially, the surface displacements are increasing with a slope of about 43 ± 2 pm/V, which can be interpreted as the domain reorientation. Then, the slope of the displacement curve decreases and subsequently saturates with increasing electric field, inducing a maximum strain level of approximately 0.025% at 10 kV/mm. In addition, there is a small hysteresis in the piezoelectric response, which is attributed to the hysteretic nature of domain motion. To verify that the displacement is not affected by electric field induced cantilever deformation, a layer of silicon wafer, which is nonferroelectric, is tested with the same method and shows no displacement under the electric field (Figure 6e). Note that the measured electromechanical coupling of the $BaTiO_3$ nanowire is close to that of high-purity, free-standing, single-crystal $BaTiO_3$ nanowires (45 pm/V)[54] and is significantly higher than ZnO nanowires (7.5 pm/V) which have found numerous applications.[27,55,56] Therefore, it indicates that the $BaTiO_3$ nanowire arrays are successfully converted from TiO_2 and are a good candidate to replace ZnO nanowire arrays in energy-harvesting and sensing devices. Furthermore, it must be emphasized that this refined PFM testing method can reduce uncertainty in measurements by at least 80% and can be easily applied in the AFM system without adding any additional components and generally without PFM capability, which shows a promising potential to be applied in the nanoscale characterization of other ferroelectric materials.

CONCLUSION

In summary, this study has demonstrated the growth of vertically aligned $BaTiO_3$ nanowire arrays on FTO glass through a novel two-step hydrothermal reaction. The vertically aligned $BaTiO_3$ nanowire arrays can be successfully converted from aligned TiO_2 nanowire arrays by the dissolution of TiO_2 and the growth of the $BaTiO_3$. The entire synthesis process is carried out with low cost equipment, which provides the potential to scale up the fabrication process of these vertically aligned ferroelectric nanowires. The piezoelectric coupling

coefficient of the $BaTiO_3$ nanowires in the longitude direction was measured to be 43 ± 2 pm/V which will allow its application in nanodevices and energy-harvesting systems. The nanowire growth process provides the potential for growth over large areas and at precisely defined locations by selectively coating FTO or Ti, which can help to achieve higher device performance. Additionally, the refined PFM testing method shows the ability to improve the accuracy of measurement, which opens a new pathway to accurately characterize nanoscale ferroelectric materials.

AUTHOR INFORMATION

Corresponding Author

*E-mail: hsodano@ufl.edu.

Notes

The authors declare no competing financial interest.

ACKNOWLEDGMENTS

The authors thank support from the Air Force Office of Scientific Research and the direction of Dr. B.L. Lee.

REFERENCES

(1) Tressler, J. F.; Alkoy, S.; Newnham, R. E. *J. Electroceram.* **1998**, *2*, 257−272.
(2) Mossi, K. M.; Selby, G. V.; Bryant, R. G. *Mater. Lett.* **1998**, *35*, 39−49.
(3) Uchino, K. In *Piezoelectric actuators and ultrasonic motors*; Springer: New York, 1996; Vol. *1*.
(4) Damjanovic, D.; Newnham, R. *J. Intell. Mater. Syst. Struct.* **1992**, *3*, 190−208.
(5) Uchino, K. In *Ferroelectric devices*; CRC: Boca Raton, FL, 2000; Vol. *16*.
(6) Muralt, P. *J. Micromech. Microeng.* **2000**, *10*, 136−146.
(7) Cook-Chennault, K.; Thambi, N.; Sastry, A. *Smart Mater. Struct.* **2008**, *17*, 043001.
(8) Priya, S. *J. Electroceram.* **2007**, *19*, 167−184.
(9) Cha, S.; Kim, S. M.; Kim, H.; Ku, J.; Sohn, J. I.; Park, Y. J.; Song, B. G.; Jung, M. H.; Lee, E. K.; Choi, B. L.; Park, J. J.; Wang, Z. L.; Kim, J. M.; Kim, K. *Nano Lett.* **2011**, *11*, 5142−5147.
(10) Wu, J.; Wang, J.; Xiao, D.; Zhu, J. *ACS Appl. Mater. Interfaces* **2011**, *3*, 3261−3263.
(11) Zhang, S.; Han, M.; Zhang, J.; Li, Y.; Hu, Z.; Chu, J. *ACS Appl. Mater. Interfaces* **2013**, *5*, 3191−3198.
(12) Liang, W.; Ji, Y.; Nan, T.; Huang, J.; Bi, Z.; Zeng, H.; Du, H.; Chen, C.; Jia, Q.; Lin, Y. *ACS Appl. Mater. Interfaces* **2012**, *4*, 2199−2203.
(13) Wu, J.; Wang, J.; Xiao, D.; Zhu, J. *Electrochem. Solid-State Lett.* **2011**, *14*, G57−G59.
(14) Tang, H.; Lin, Y.; Andrews, C.; Sodano, H. A. *Nanotechnology* **2011**, *22*, 015702.
(15) Datta, A.; Mukherjee, D.; Hordagoda, M.; Witanachchi, S.; Mukherjee, P.; Kashid, R. V.; More, M. A.; Joag, D. S.; Chavan, P. G. *ACS Appl. Mater. Interfaces* **2013**, *5*, 6261−6267.
(16) Liu, M.; Li, X.; Imrane, H.; Chen, Y.; Goodrich, T.; Cai, Z.; Ziemer, K. S.; Huang, J. Y.; Sun, N. X. *Appl. Phys. Lett.* **2007**, *90*, 152501.
(17) Son, J. Y.; Lee, J.; Song, S.; Shin, Y.; Jang, H. M. *ACS Nano* **2013**, *7*, 5522−5529.
(18) Narayanan, T. N.; Mandal, B. P.; Tyagi, A. K.; Kumarasiri, A.; Zhan, X.; Hahm, M. G.; Anantharaman, M. R.; Lawes, G.; Ajayan, P. M. *Nano Lett.* **2012**, *12*, 3025−3030.
(19) Zhu, Y.; Zhang, L.; Natsuki, T.; Fu, Y.; Ni, Q. *ACS Appl. Mater. Interfaces* **2012**, *4*, 2101−2106.
(20) Szwarcman, D.; Vestler, D.; Markovich, G. *ACS Nano* **2011**, *5*, 507−515.
(21) Hochbaum, A. I.; Yang, P. *Chem. Rev.* **2010**, *110*, 527−546.
(22) Jung, J. H.; Lee, M.; Hong, J.; Ding, Y.; Chen, C.; Chou, L.; Wang, Z. L. *ACS Nano* **2011**, *5*, 10041−10046.
(23) Xu, S.; Yeh, Y.; Poirier, G.; McAlpine, M. C.; Register, R. A.; Yao, N. *Nano Lett.* **2013**, *13*, 2393−2398.
(24) Lin, Y.; Liu, Y.; Sodano, H. A. *Appl. Phys. Lett.* **2009**, *95*, 122901.
(25) Zhang, X.; Zhao, X.; Lai, C.; Wang, J.; Tang, X.; Dai, J. *Appl. Phys. Lett.* **2004**, *85*, 4190−4193.
(26) Varghese, J.; Barth, S.; Keeney, L.; Whatmore, R. W.; Holmes, J. D. *Nano Lett.* **2012**, *12*, 868−872.
(27) Wang, Z. L.; Song, J. *Science* **2006**, *312*, 242−246.
(28) Liu, J.; Wu, W.; Bai, S.; Qin, Y. *ACS Appl. Mater. Interfaces* **2011**, *3*, 4197−4200.
(29) Xu, S.; Hansen, B. J.; Wang, Z. L. *Nature Commun.* **2010**, *1*, 93.
(30) Zlotnik, S.; Vilarinho, P. M.; Costa, M. E.; Agostinho Moreira, J.; Almeida, A. *Cryst. Growth Des.* **2010**, *10*, 3397−3404.
(31) Haertling, G. H. *J. Am. Ceram. Soc.* **1999**, *82*, 797−818.
(32) Limmer, S. J.; Seraji, S.; Wu, Y.; Chou, T. P.; Nguyen, C.; Cao, G. Z. *Adv. Funct. Mater.* **2002**, *12*, 59−64.
(33) Huang, K.; Huang, T.; Hsieh, W. *Inorg. Chem.* **2009**, *48*, 9180−9184.
(34) Teresa Buscaglia, M.; Harnagea, C.; Dapiaggi, M.; Buscaglia, V.; Pignolet, A.; Nanni, P. *Chem. Mater.* **2009**, *21*, 5058−5065.
(35) Urban, J. J.; Yun, W. S.; Gu, Q.; Park, H. *J. Am. Chem. Soc.* **2002**, *124*, 1186−1187.
(36) Chen, Y. Z.; Liu, T. H.; Chen, C. Y.; Liu, C. H.; Chen, S. Y.; Wu, W. W.; Wang, Z. L.; He, J. H.; Chu, Y. H.; Chueh, Y. L. *ACS Nano* **2012**, *6*, 2826−2832.
(37) Rørvik, P. M.; Almli, Å; van Helvoort, A. T. J.; Holmestad, R.; Tybell, T.; Grande, T.; Einarsrud, M. A. *Nanotechnology* **2008**, *19*, 225605.
(38) Rørvik, P. M.; Grande, T.; Einarsrud, M. A. *Cryst. Growth Des.* **2009**, *9*, 1979−1984.
(39) Liu, B.; Aydil, E. S. *J. Am. Chem. Soc.* **2009**, *131*, 3985−3990.
(40) Begg, B. D.; Vance, E. R.; Nowotny, J. *J. Am. Ceram. Soc.* **1994**, *77*, 3186−3192.
(41) Chien, A.; Xu, X.; Kim, J.; Sachleben, J.; Speck, J.; Lange, F. *J. Mater. Res.* **1999**, *14*, 3330−3339.
(42) Cho, C.; Shi, E.; Jang, M.; Jeong, S.; Kim, S. *Jpn. J. Appl. Phys.* **1994**, *33*, 4984−4990.
(43) Eckert, J. O.; Hung-Houston, C. C.; Gersten, B. L.; Lencka, M. M.; Riman, R. E. *J. Am. Ceram. Soc.* **1996**, *79*, 2929−2939.
(44) Kang, S.; Park, B. H.; Kim, Y. *Cryst. Growth Des.* **2008**, *8*, 3180−3186.
(45) Xu, H.; Gao, L. *Mater. Lett.* **2002**, *57*, 490−494.
(46) Pinceloup, P.; Courtois, C.; Vicens, J.; Leriche, A.; Thierry, B. *J. Eur. Ceram. Soc.* **1999**, *19*, 973−977.
(47) Zhou, Z.; Lin, Y.; Tang, H.; Sodano, H. A. *Nanotechnology* **2013**, *24*, 095602.
(48) Bang, J. H.; Kamat, P. V. *Adv. Funct. Mater.* **2010**, *20*, 1970−1976.
(49) Wang, G.; Wang, H.; Ling, Y.; Tang, Y.; Yang, X.; Fitzmorris, R. C.; Wang, C.; Zhang, J. Z.; Li, Y. *Nano Lett.* **2011**, *11*, 3026−3033.
(50) Wang, J.; Sandu, C.; Setter, N. *IEEE Trans. Ultrason., Ferroelectr., Freq. Control* **2009**, *56*, 1813−1819.
(51) Wang, Z.; Hu, J.; Yu, M. *Appl. Phys. Lett.* **2006**, *89*, 263119.
(52) Wang, Z.; Hu, J.; Yu, M. *Nanotechnology* **2007**, *18*, 235203.
(53) Lin, Y.; Sodano, H. A. *Adv. Funct. Mater.* **2009**, *19*, 592−598.
(54) Wang, Z.; Hu, J.; Suryavanshi, A. P.; Yum, K.; Yu, M. *Nano Lett.* **2007**, *7*, 2966−2969.
(55) Fan, H. J.; Lee, W.; Hauschild, R.; Alexe, M.; Le Rhun, G.; Scholz, R.; Dadgar, A.; Nielsch, K.; Kalt, H.; Krost, A. *Small* **2006**, *2*, 561−568.
(56) Wang, X.; Wang, X.; Summers, C. J.; Wang, Z. L. *Nano Lett.* **2004**, *4*, 423−426.